Proceedings of ASME Turbo Expo 2014: Turbine Technical Conference and Exposition
GT2014
June 16 – 20, 2014, Düsseldorf, Germany

GT2014-26478

INVESTIGATION OF A COMPRESSOR ROTOR NON-SYNCHRONOUS VIBRATION WITH AND WITHOUT FLUID-STRUCTURE INTERACTION

Jiaye Gan *
Hong-sik Im †
Daniel Espinal, Alexis Lefebvre
Ge-Cheng Zha ‡
Dept. of Mechanical and Aerospace Engineering
University of Miami
Coral Gables, Florida 33124
E-mail: gzha@miami.edu

Nomenclature

BC	Boundary Condition
CUSP	Convective Upwind and Splitting Pressure
DES	Detached Eddy Simulation
DDES	Delayed Detached Eddy Simulation
FSI	Fluid-structural interaction
IGV	Inlet Guide Vane
NSV	Non-Synchronous Vibration
RI	Rotating Instability
SFV	Separated Flow vibration
URANS	Unsteady Reynolds-Averaged Navier-Stokes
WENO	Weighted Essentially Non-Oscillatory

ABSTRACT

This paper study the non-synchronous vibration (NSV) of a high speed multistage axial compressor using rigid blade and vibrating blade with fluid-structural interaction(FSI). The unsteady Reynolds-averaged Navier-Stokes (URANS) equations and mode based structural dynamic equations are solved. A low diffusion E-CUSP Reimann solver with a 3rd order WENO scheme for the inviscid fluxes and a 2nd order central differencing for the viscous terms are employed. A $1/7$th annulus sector of IGV-rotor-stator is used with a time shifted phase lag BC at circumferential boundaries. An interpolation sliding boundary condition is used for the rotor-stator interaction. The URANS simulation for rigid blades shows that the leading edge(LE) tornado vortices, roughly above 80% rotor span, travel backwards relative to the rotor rotation and cause an excitation with the frequency agreeing with the measured NSV frequency. The predicted excitation frequency of the traveling vortices in the rigid blade simulation is a non-engine order frequency of 2603 Hz, which agrees very well with the NSV rig testing. For the FSI simulation, the results show that there exist two dominant frequencies in the spectrum of the blade vibration. The lower dominant frequency is close to the first bending mode. The higher dominant frequency close to the first torsional mode agrees very well with the measured NSV frequency . The simulation conducted in this paper appears to indicate that the NSV is excited by the traveling vortex.

1 Introduction

Blade vibration due to forced response and flutter have been studied for decades with the progress of improving turbomachinery efficiency and reliability. Recently, a new turbomachinery aeromechanic problem, namely non-synchronous vibration(NSV), whose blade vibration frequency is away from harmonics of rotor shaft frequency, has attracted a lot of attention [1–9]. The high speed axial compressor investigated in this study exhibits such an non-engine order vibration on the 1st stage rotor blades during the engine acceleration in the rig testing [2,9,10] as shown in Fig. 1, i.e. non-synchronous vibration (NSV). The NSV frequency collapses between 2600 Hz and 2661 Hz with a large amplitude close to the blade 1T (1st torsional) mode. Im and Zha [9]

*ASME Member, Ph.D. Student
†ASME Member, Ph.D. Currently an engineer at Honeywell
‡Professor, ASME Fellow

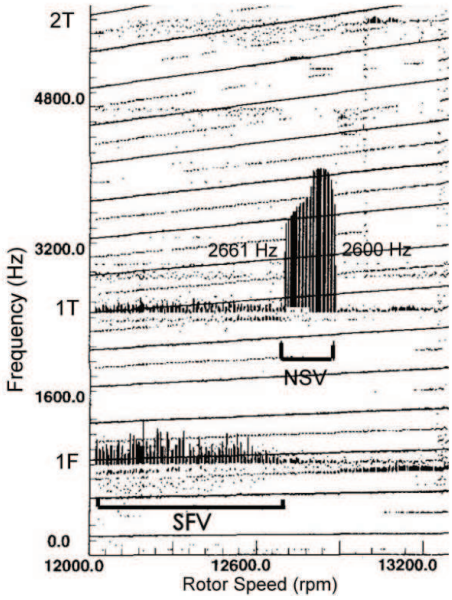

FIGURE 1: Strain gage response of the first-stage rotor blades of a high-speed compressor showing the frequency lock-in near the 1st torsional mode (1T) during the NSV

simulated the GE 1-1/2 stage compressor with rigid blade and discovered that the tangential traveling vortex matches the NSV excitation frequency. No rotating stall is observed when the NSV occurs.

A propagating vortex structure near the blade tip in a low speed axial compressor is also reported in [4] as a rotating instability (RI) that causes the axial compressor NSV. Their measurements show that the RI is limited to the blade tip region with the peak amplitude at 92% of the blade height around 20% to 30% of the chord and it travels in the opposite direction to rotor rotation. Similarly, the experiment for a 10 stage high pressure axial compressor [1] shows a NSV of the 1st stage rotor blades due to a RI. The measured frequencies indicate radial dependency of the NSV with high coherence above 74% rotor span, which decays away from the RI and is eventually no more detectable below 65% blade span.

Thomassin, et al. [5,6] suggested a theory different from the rotating instability to explain the NSV based on the resonance of a impinging jet vortex structure and the acoustic feedback of a vibrating plate. The jet core feedback theory has been proved by an experiment conducted in [5, 6]. It shows that when the acoustic reflection wave length equals to the jet-to-plate distance, the jet vortical structures lock-on to the acoustic wave frequency and significant amplification of the pressure fluctuation and vibration of the flexible plate are observed. They suggest a simple model to predict the critical tip velocity based on their impinging jet experiment. Vo's [8] simulation shows a tip clearance flow instability for an isolated subsonic axial compressor rotor. In the blade tip region the trailing edge back flow causes flow impingement on the pressure side that leads to the flow unsteadiness associated with the NSV.

Recently, Clark et al. [11] introduce the classical Van Der Pol oscillator to analogize the NSV phenomenon in turbomachinery. They consider the NSV as a phase lock phenomenon that the flow vortex shedding locks in with a structural mode frequency with a range.

The purpose of this paper is to further investigate the NSV mechanism by comparing the flow excitation with rigid blades and the blade vibration with fluid-structural interaction. The same GE 1-1/2 stage compressor is simulated under the rig testing NSV condition with rigid and vibrating blades. If the phase locking phenomenon is the NSV cause as suggested by Clark et al. [11], the rigid blades simulation may have no excitation frequency matching the NSV frequency since the blades are not vibrating. The present study captures the NSV excitation from the tangentially traveling wave with and without blade vibration. The simulations appear to indicate that the NSV of this compressor rotor is excited by the unsteady aerodynamic forcing instead of phase locked to the structural frequency. However, this my not be conclusive since a more strict study should also vary the RPM within a range to see if the NSV exists with a frequency range as shown in Fig. 1.

2 Numerical Models

For the fully coupled FSI method used in this study [10], time accurate 3D compressible Navier-Stokes equations are solved with a system of 5 decoupled modal equations in a fully coupled manner. For rigid blade simulation, the structural solver was switched off. The URANS equations are solved in a rotating frame with the Spalart-Allmaras (SA) turbulence model [12]. Shock capturing scheme is necessary to simulate high-speed axial compressors since most rotor blades experience shock/boundary layer interaction. In this study the Low Diffusion E-CUSP (LDE) Scheme [13] as an accurate shock capturing Riemann solver is used with a 3rd order WENO reconstruction for inviscid flux and a 2nd order central differencing for viscous terms [14]. An implicit 2nd order dual time stepping method [15] is solved using an unfactored Gauss-Seidel line iteration to achieve high convergence rate. The high-scalability parallel computing is implemented to save wall clock time [16]. For fully coupled FSI, the flow field and structure always respond simultaneously by exchanging the unsteady aerodynamic force and structural displacement within each physical time step via a successive iteration on the pseudo-time step. In this study, a robust deforming mesh generation technique [17] that can significantly reduce mesh skewness at the rotor tip clearance is used.

An efficient time-shifted BC [9] is implemented and applied at lower/upper circumferential periodic boundaries to facilitate 1/7th annulus simulations. Five nodal diameter observed in the rig test is used in the simulation. At the IGV inlet, the radial distributions of total pressure, total temperature, swirl angle and pitch angle from experimental data are specified and velocity is extrapolated from the computational domain in order to determine the rest of the variables. On the blade surface a non-slip boundary condition is utilized, while an efficient wall function BC [18] is used on the hub/casing

surface where y^+ is greater than 11 to avoid an excessive fine mesh in the boundary layer. At the stator outlet, the static pressure from experimental data is specified in the spanwise direction. The velocity components are extrapolated from the computational domain and an isentropic relation is used to determine density. The hub/casing wall static pressure for the inviscid momentum equation is determined by solving the radial equilibrium equation, whereas the static pressure gradient across the wall boundary is set to zero for the blade wall surface. An adiabatic condition is used to impose zero heat flux through the wall.

3 Simulation of the Compressor NSV without FSI

The rig testing axial compressor shows a NSV around 2600 Hz to 2661 Hz, i.e. non-engine order vibration between 12EOL(engine order line) to 13EOL as shown in the Campbell diagram in Fig. 2. The experimental operating condition taken by the present simulation is a NSV of 2600 Hz at 12880 RPM. The residual is reduced by three orders of magnitude within each physical time step, which is usually achieved within 30 to 40 pseudo time step iterations. A non-dimensional time step of about 0.005 is used. The NSV frequency predicted by the current URANS simulation is 2603 Hz, which excellently agrees with the experiment as shown in Campbell diagram in Fig. 2. Note that unsteady solutions over 6 rotor revolutions was obtained for total 168 hours with 168 CPUs computing by using Air Force Research Lab DoD High Performance Computing Resources.

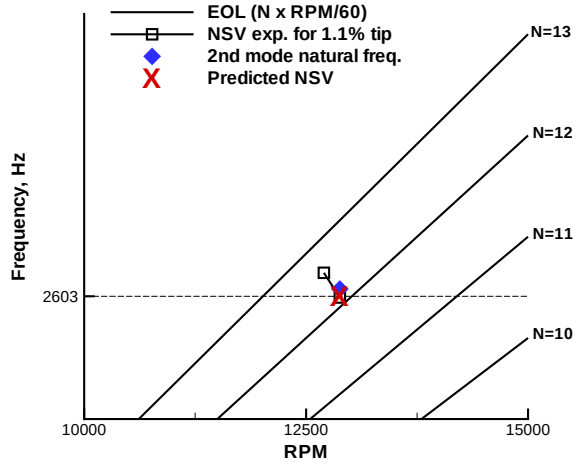

FIGURE 2: Campbell diagram for the high speed compressor near NSV, where N represents order of engine harmonics

3.1 Computational Mesh

The 1-1/2 stage of the GE-C1 compressor studied in this paper has 56 IGV blades, 35 rotor blades and 70 stator blades. To save computational time, a 1/7th annulus sector was simulated. The mesh of the sector used in this study is presented in Fig. 3. The mesh around IGV/rotor/stator blades was constructed using the O-mesh. For the IGV and stator, 121 (around blade)×101 (blade-to-blade)×71 (blade span) is the mesh size, and for the rotor, 201 (around blade)×101 (blade-to-blade)×71 (blade span). The mesh on the two sides of rotor-stator interface can be arbitrary in the circumferential direction since an interpolation technique is used to calculate the fluxes across the interface. The rotor tip clearance is modeled with 21 grid points across the clearance gap using an O-mesh block as shown in Fig. 3 (middle). The 1-1/2 stage mesh is partitioned into total 168 blocks for parallel computation. Total mesh size used for the compressor NSV simulation is 11,968,848. The mesh refinement study [9] shows that the unsteady flow solution is converged based on the current mesh size.

Since NSV of axial compressors is typically observed in stable operation [1–4], unsteady flow simulations are first conducted with rigid blades and no vibration mesh at different back pressure conditions to find NSV dominant region in the speedline.

Fig. 4 shows the predicted speedline of the 1-1/2 stage axial compressor. Note that the speedline data based on the fine mesh in Fig. 4 are obtained by averaging final 2 rotor revolutions to avoid the transitional period since the unsteady computations are started from the steady solutions obtained by a mixing plane approach [19]. The point A, B, C and D represent rotor-to-IGV total pressure characteristics. The back pressure is gradually increased from the point S to find the near stall point D. After the point D the compressor is stalled. The point S is about maximum mass flow condition. No NSV excitations are found at point S. The mass flow rate obtained at the point C is about 6% lower than the near stall point D. The peak NSV excitation frequency of 2603 Hz is observed at the point C, which excellently agrees with the rig testing NSV of 2600 Hz. The total pressure ratio changed between point C and FSI may be because the simulation without FSI overestimates the viscous flow losses and flow deviation with mixing plane method.

Fig. 5 shows time history of the rotor outlet mass flow rate predicted by the fully coupled FSI. In this study the unsteady solutions after one rotor revolutions are used for NSV frequency analysis since the predicted mass flow shows periodic oscillations.

3.2 The LE tornado vortex

Fig. 6 shows instantaneous entropy ($\frac{\Delta S}{R} = \frac{\gamma}{\gamma-1} ln \frac{To}{To_\infty} - ln \frac{Po}{Po_\infty}$) near the rotor LE axial plane. The flow above 80% blade span is largely disturbed due to a tornado vortex that triggers the non-engine order vibration of the compressor. The NSV with large blade vibration amplitude is attributed to the tornado vortex travelling in the circumferential direction between 65% to 91% of the blade span.

The LE tornado vortex captured for this compressor roughly above 80% rotor span is the travelling vortex as illustrated in Fig. 7. V1, V2, V3, V4, V5 indicates the vortex

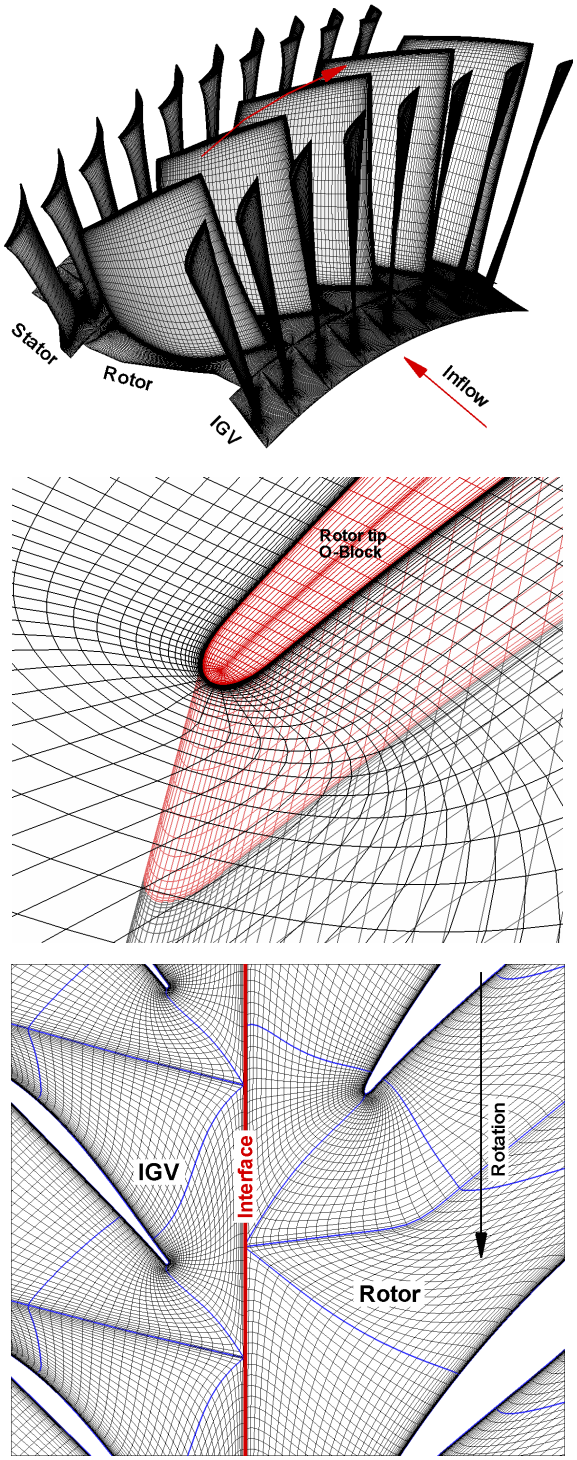

FIGURE 3: 1/7th annulus sector mesh of 1-1/2 stage axial compressor; 3D blade (top), tip block (middle), blade-to-blade (bottom)

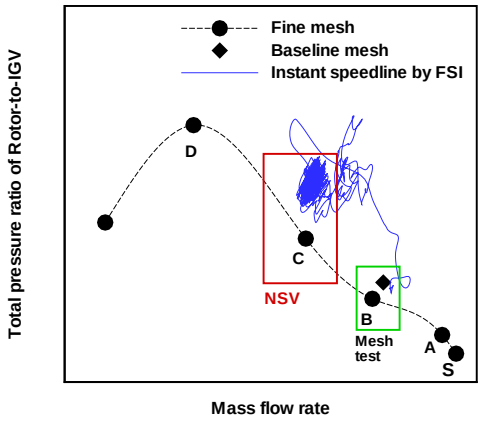

FIGURE 4: IGV-to-rotor speedline from the fully coupled FSI

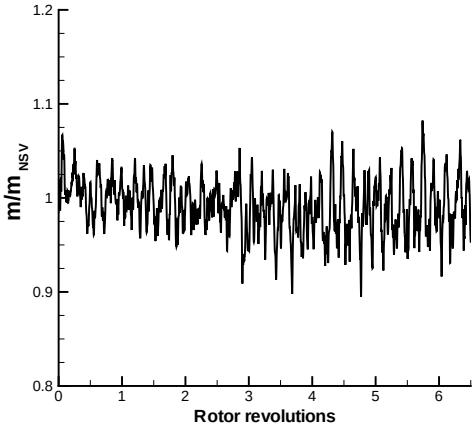

FIGURE 5: Instantaneous mass flow during NSV from the fully coupled FSI

core around blade 1, 2, 3, 4, and 5, respectively. Unlike the regular streamwise tip clearance vortex, it swirls with vortex axis normal to the blade suction surface like a tornado vortex and travels counter to the rotor rotation direction. As indicated in [9], the tip vortex travels from a blade LE to trailing edge and then to the LE of the next blade. Such a vortex motion generates a pair of aerodynamic excitation for blade torsional vibration because of two low pressure regions followed by the vortex core positions, one near the LE and one near the trailing edge.

Fig. 8 indicates the reversal flow near the rotor tip region due to the tornado vortices travelling. A locally stalled flow appears near the rotor tip, but no rotating stall happens during the compressor NSV. The tornado vortex is examined at time T1, T1+Δt and T1+2Δt, where Δt is about 0.045 Rev (rotor revolutions). Fig. 9 shows instantaneous movement of the tornado vortex V2 at t=T1, T1+Δt, T1+2Δt. It is obvious that the vortex instability travels in the opposite direction to the rotor rotation near the rotor LE upstream, e.g. the tornado vortex V2 seen near LE suction surface of blade 2 at t=T1 is moved to blade 3 LE at T=T1+2Δt.

As another evidence of the tornado vortices travelling, the normalized static pressure distributions on the rotor blade

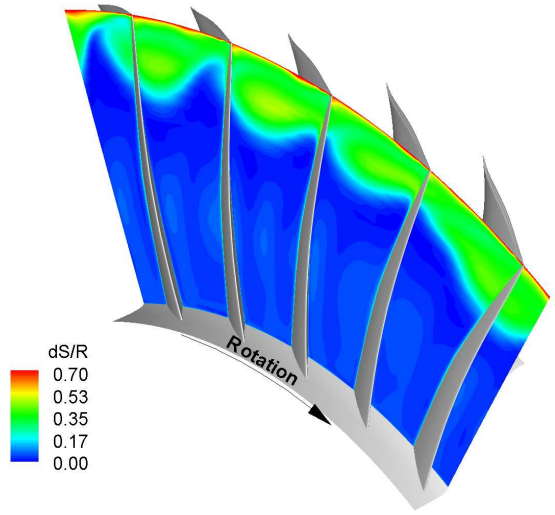

FIGURE 6: Entropy contour near the rotor LE axial plane

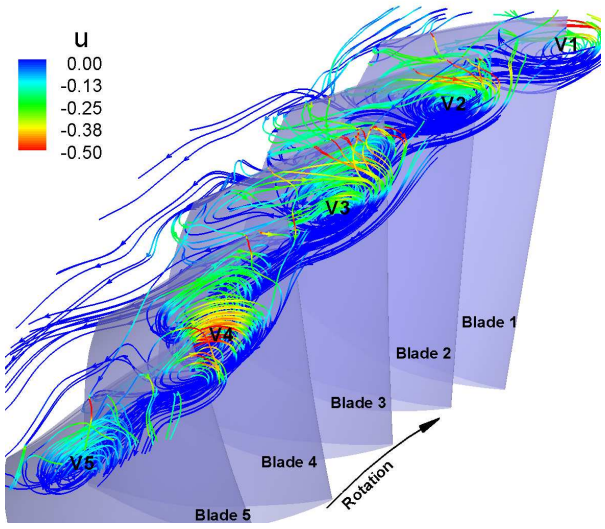

FIGURE 7: Structure of the LE tornado vortex causing NSV above 80% rotor span colored by negative axial velocity

surface near 90% span are plotted in Fig.n10 and Fig. 11. The low pressure regions represent the core of tornado vortices. For example, V1 core near 10% axial chord at t=T1 moves to about 20% axial chord at t=T1+Δt. At t=T1, two vortex cores simultaneously appear on the blade passage 5 due to the vortex leaving and coming, e.g. see V4 and V5 in Fig. 7.

3.3 Propagating Frequency of the LE tornado vortex

The static pressure signals are acquired for the frequency analysis from total 60 numerical probes mounted on a blade surface including tip clearance. The peak fluctuations among those acquired pressure signals are observed around 80% span near the rotor LE due to the travelling tornado vortices as plotted in Fig. 12. Such a pressure oscillation due

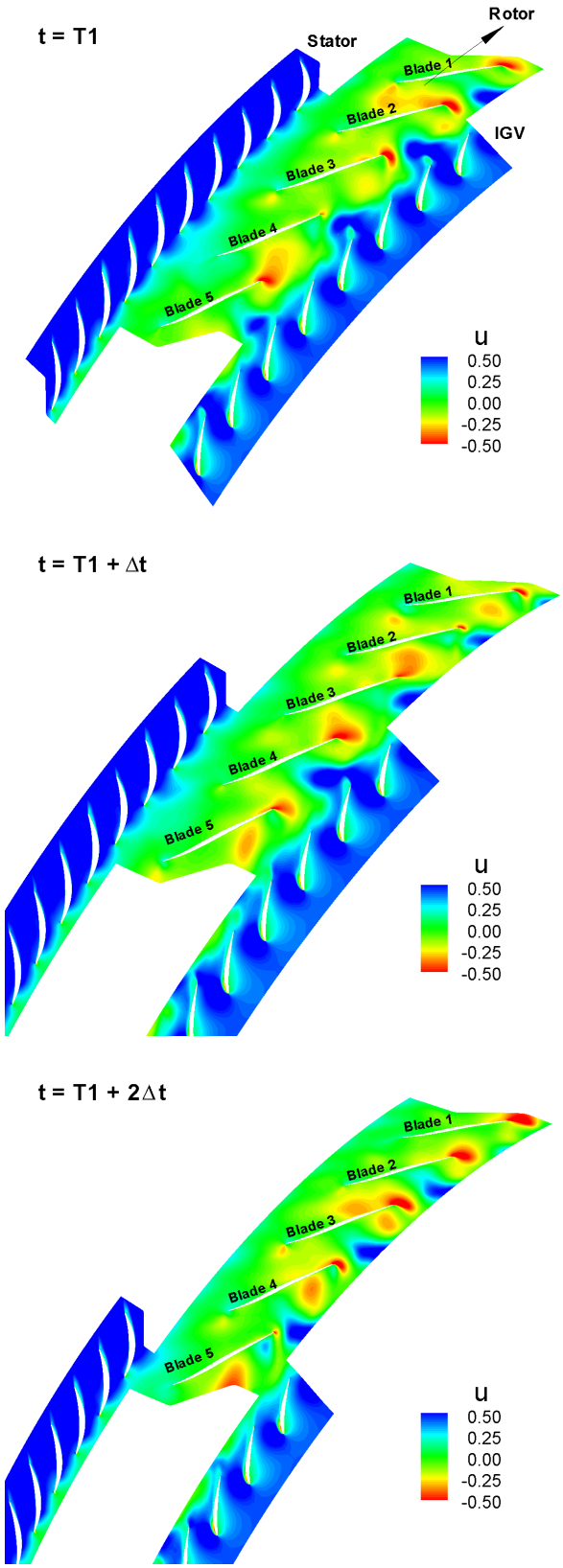

FIGURE 8: Axial velocity (u) contour near the blade tip section

to the travelling vortex generates a severe aerodynamic excitation, and which results in the NSV of the high speed axial

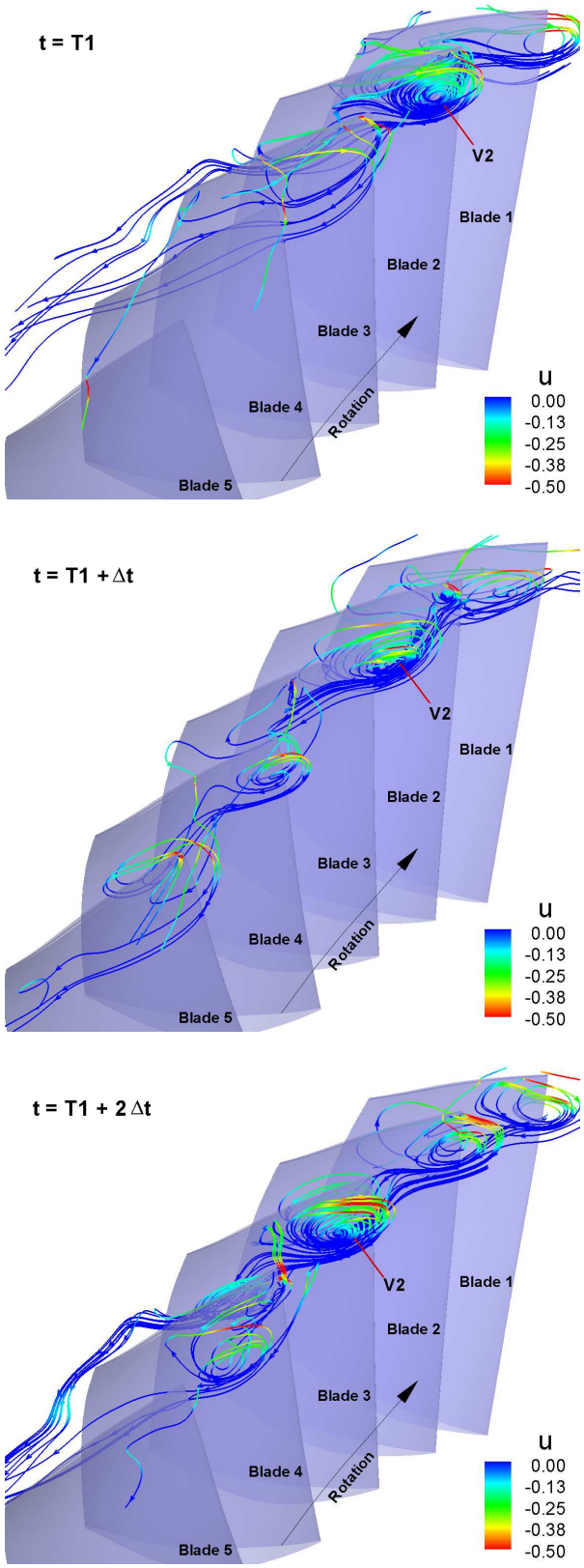

FIGURE 9: Movement of the travelling vortex V2 in the backwards to the rotor rotation at t=T1, T1+Δ*t*, T1+2Δ*t* during the NSV

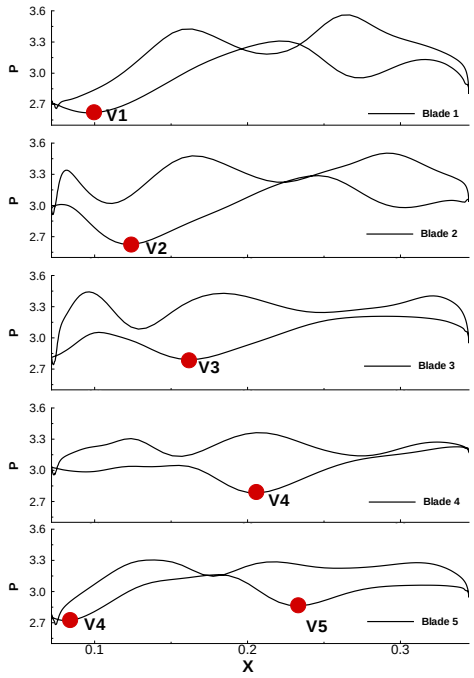

FIGURE 10: Normalized static pressure around the blade surface near 90% rotor span at T1

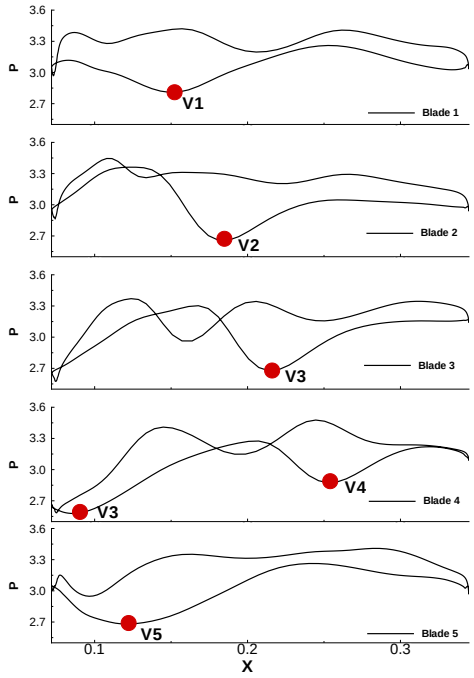

FIGURE 11: Normalized static pressure around the blade surface near 90% rotor span at T1+Δ*t*, where Δ*t* is about 0.045 Rev

compressor as identified from the frequency analysis in Fig. 13. The total sampling time is about 7 rotor revolutions with more than 2048 samples. The frequency resolution is about 30 Hz. The predicted dominant NSV excitation frequency is 2603 Hz, which agrees excellent with the measured NSV

frequency of 2600 Hz in the rig testing given in Fig. 1.

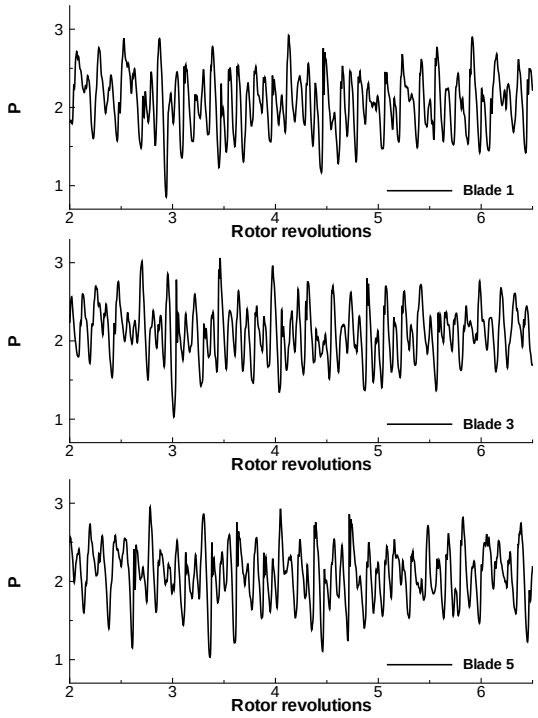

FIGURE 12: Normalized static pressure signal acquired near 80% span rotor LE

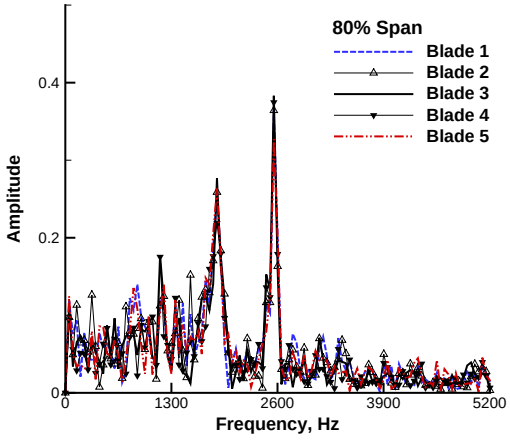

FIGURE 13: Predicted frequencies using the normalized static pressure signal near 80% span rotor LE

4 Simulation of compressor with FSI

The fluid-structural interaction simulation starts from the unsteady results of the rigid blades with the blades allowed governed by the modal structure equations. The first five mode shapes used in this study can be found in [10]. And the natural frequencies of the five modes are 1065.5 Hz, 2621.0 Hz, 3591.0 Hz, 5275.4 Hz, 6226.4 Hz, respectively. The natural frequencies are from blade alone finite element analysis. In practice, it is difficult to get the structural damping. In current simulation, the structural damping is assumed to be zero. Hence, the damping of the response only contain the aerodynamic damping. The rig testing of the full axial compressor with 1.1% tip clearance is observed with the NSV frequency range from 2600 Hz to 2661 Hz, which is located between 12 EOL to 13 EOL and is near the second mode or the first torsional mode(1T). The conditions used for the present NSV simulation correspond to the operating conditions at the rig test with the NSV frequency at 12880 RPM.

Fig. 14 and Fig. 15 show the first three modal displacements of each blades. As shown in Fig. 14 and Fig. 15, the second mode amplitude captured in this simulation has a linear growth until about 11 rotor revolutions and becomes flat after that. This is a typical limited cycle oscillation (LCO), which is the NSV observed in the compressor rig test with the same frequency to be shown later. However, Fig. 14 and Fig. 15 clearly show that the responses of the first mode of all blades linearly grows until 4.5 revolutions, then the amplitude becomes dynamically stable as LCO, which is also a sign of NSV. The first mode amplitude is also significantly greater than the second mode. Interestingly, the unsteady flow simulation with rigid blade does not capture a strong excitation near the first mode frequency as shown in Fig. 13. It is clearly seen in Fig. 14 and Fig. 15 that the responses of the third mode are small and damped out with time. Although the amplitudes of the first mode of the five blades are different, the time average of amplitudes are about the same for all the blades.

Fig. 16 shows the net tangential physical displacement at the rotor tip LE, where y0,z0 denotes y-,z-coordinates of initial blade position. It is shown that the blade vibration is composed of more than one major modes. Frequency analysis using the tangential physical displacements at rotor tip LE in different blades is shown in Fig. 17. The predicted frequency indicates no resonance occur with blade natural frequencies during the NSV. Two dominant frequencies are observed during the NSV, which is not observed from the results of the rigid blades without FSI. The first dominant frequency is 1069 Hz, which is close to the first bending mode frequency of 1065.5 Hz. The second dominant frequency is 2602 Hz and is close to the first torsional mode frequency of 2621 Hz, and matches the NSV of the first torsional mode with frequency 2600Hz measured in the rig test very well. The amplitude of the first dominant frequency is more than 2 times greater than that of the second dominant frequency. However, the first mode NSV is not detected in the rig test. Since the FSI simulation in [10] uses the damping ratio of 0.005 and captures the 1st torsion mode NSV with the 1st

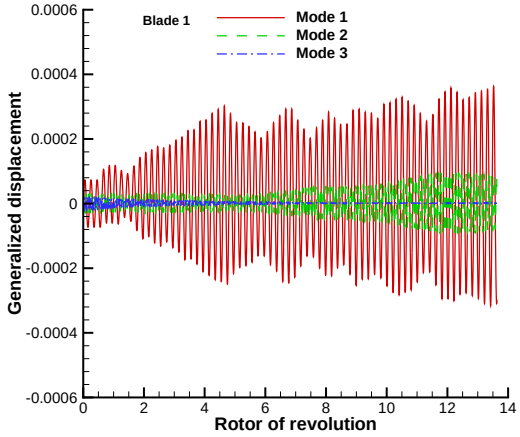

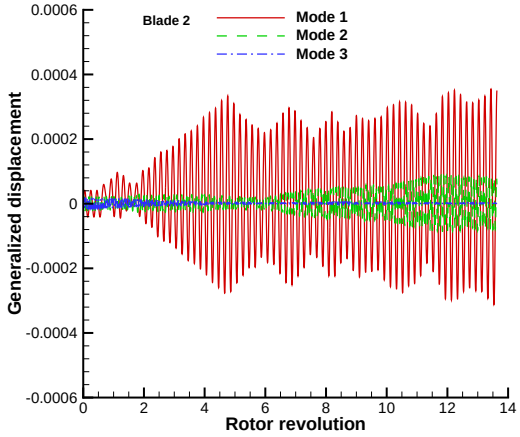

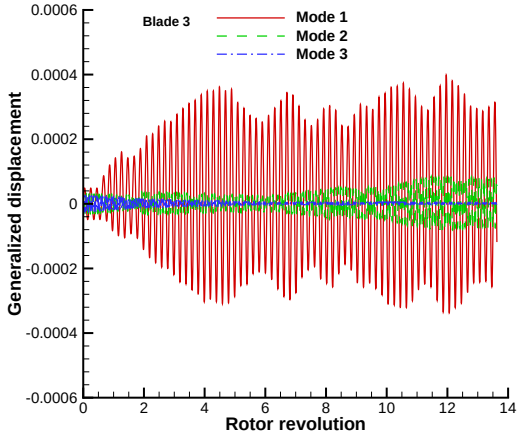

FIGURE 14: Modal displacements of the blade 1 to blade 3 during NSV from the fully coupled FSI

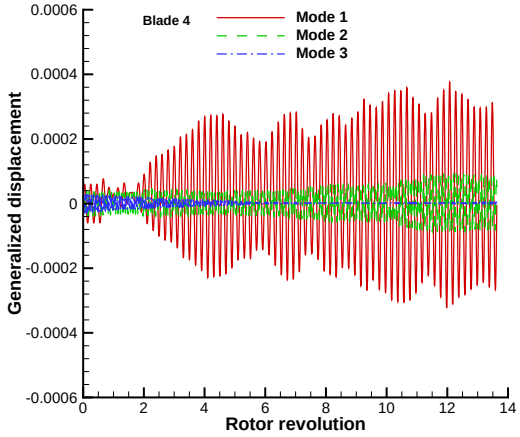

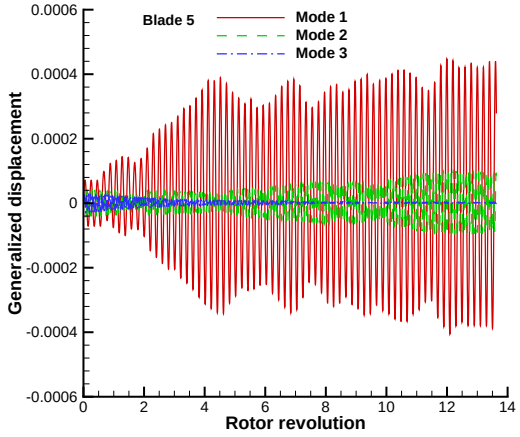

FIGURE 15: Modal displacements of the blade 4 and blade 5 during NSV from the fully coupled FSI

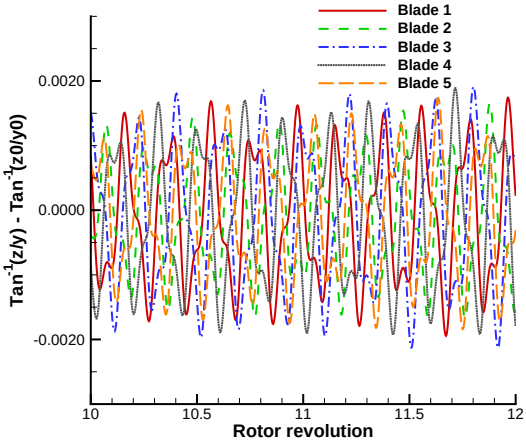

FIGURE 16: Normalized net tangential displacements at the rotor tip LE during NSV from coupled FSI

bending mode damped out, the zero damping ratio used in this simulation is may be the cause for the 1st bending mode NSV.

Spectrum analysis of instantaneous blade surface pressure at 4 different span along LE are plotted in Fig. 18. The

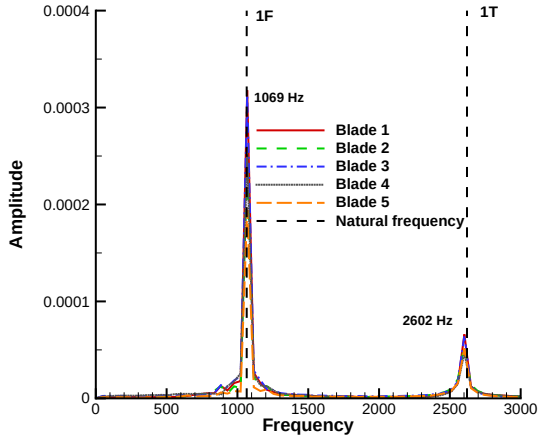

FIGURE 17: Predicted frequencies using the tip displacements from the fully coupled FSI

fluctuating characteristics are different along the spanwise. The maximum amplitude of the pressure is observed at about 80% span near LE. Several dominant frequencies are found at this location. The excitations with frequencies of 877 Hz, 1740 Hz, and 3480 Hz are engine orders. The corresponding vibrations are mainly because of the interactions between the rotor blades and the wake from the IGV blades. The excitation with frequency of 2602 Hz is a source of NSV, since the frequency is not at the engine order and is very close to the NSV frequency of 2600 Hz in experiment. The predicted NSV frequency with FSI simulation is almost the same as that of the rigid blades without FSI with 1 Hz difference. Frequencies of instantaneous displacements at 4 different span along LE are also plotted in Fig. 18. Compared with the spectrum of pressure, there are two dominant frequencies in every spectrum of displacement along the spanwise, which indicates the frequencies of vibration of the whole blade are the same but with different amplitudes at different span. The component of the first dominant blade vibrating frequency of 1069 Hz is closed to the blade passing frequency of 877 Hz, which may be the excitation. The predicted frequencies of the second displacement peaks from the 4 different span locations are the same and all equal to 2602 Hz. Note that the frequency of second peak in the displacement spectrum is the same as the peak in the pressure spectrum from the rigid blade simulation shown in Fig. 13, which indicates the vibration of the blade is driven by the flow at 2602 Hz.

More detail spectrum results are shown from Fig. 19 to Fig. 22. Fig. 19 shows the maximum amplitude contours of pressure fluctuation on the whole surface of rotor blade 4. It is clear that the location of maximum pressure fluctuation appears at the LE from 75% to 85% span. Fig.20 shows the corresponding frequency of maximum amplitude of the pressure. The frequencies that aerodynamic force acting on the blade surface would mainly be about 1730 Hz and 2600 Hz. Frequencies analysis of angular displacements on the same blade surface are shown in Fig. 21 and Fig. 22. The phys-

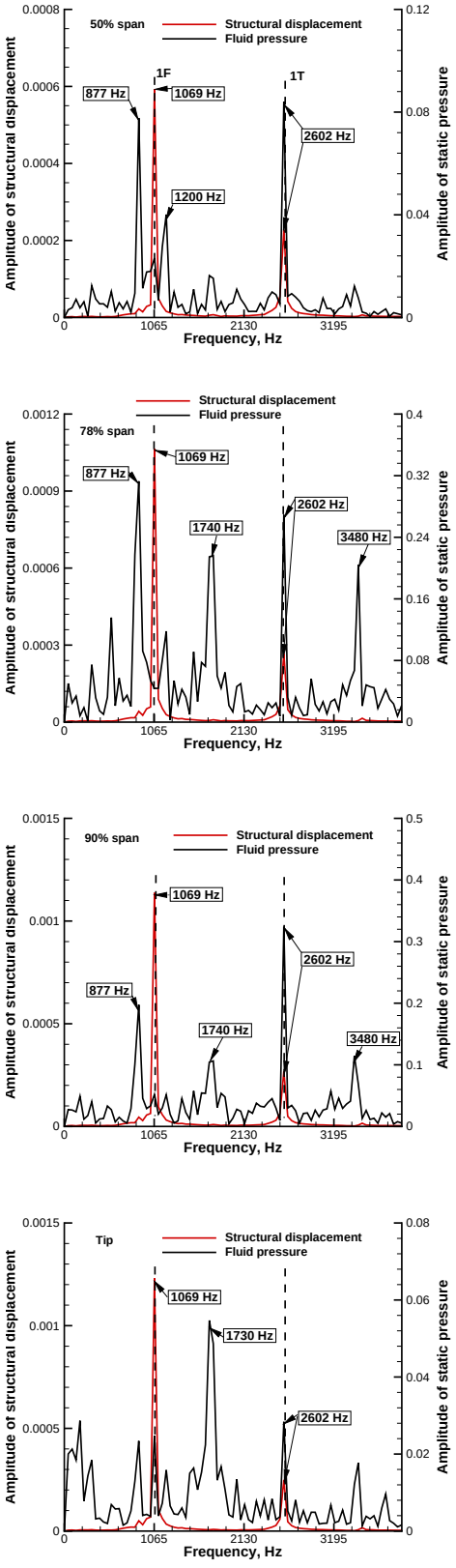

FIGURE 18: Pressure spectrum compared with that of displacement at four different spans

ical displacements are obtained based on the time history c generalized displacements of the 5 modes. The discontinu ity in contour plot is because the blade surface was split. is observed that the maximum vibration located at the tip The blade is vibrated in two mainly frequencies 1065 Hz an 2600 Hz, which can be found from Fig. 22.

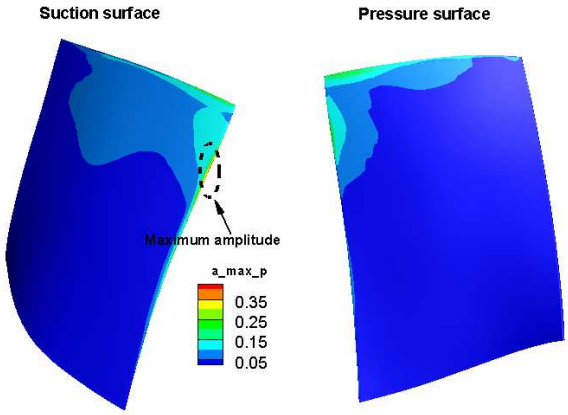

FIGURE 19: Predicted maximum amplitude contours of pressure using FFT

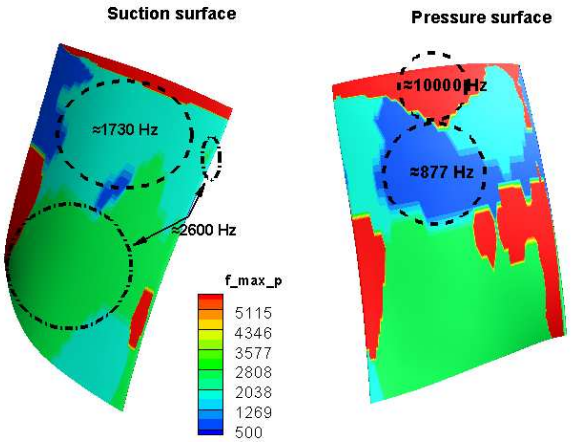

FIGURE 20: Predicted peak frequencies contours of pressure using FFT

The LE tornado vortex in captured in the rigid blade simulation is also obtained in this FSI simulation at about 80% span of the blade as shown in Fig. 23. The vortex swirls strongly with its' axis normal to the blade suction surface and travels backwards to the rotor rotation. The frequency of the vortex motion is the same as the one simulated with rigid blades and matches the NSV frequency [10].

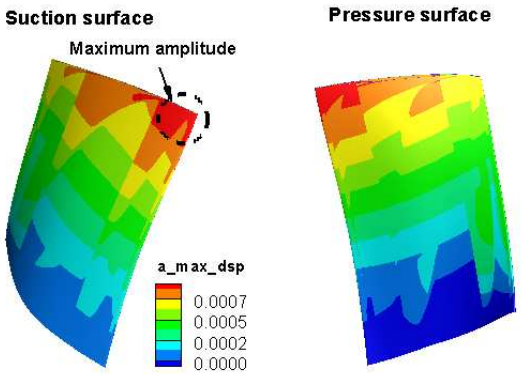

FIGURE 21: Predicted maximum amplitude contours of displacement using FFT

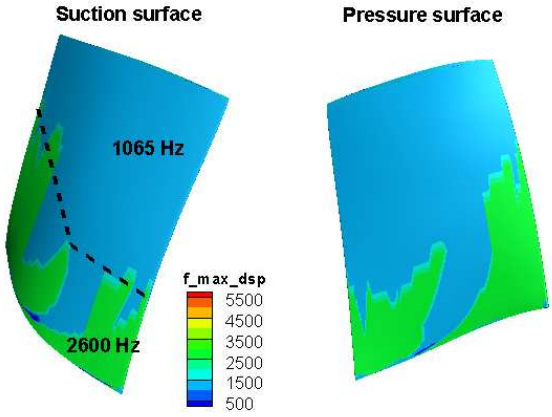

FIGURE 22: Predicted peak frequencies contours of displacement using FFT

5 Conclusion

In this study a high speed axial compressor is simulated with and without blade vibration to investigate the NSV mechanism. A 1/7th annulus sector of IGV-rotor-stator is used with a time-shifted phase lag BC at circumferential boundaries to reduce computational efforts. A sliding interpolation BC is implemented using liner interpolation in order to capture the unsteady rotor-stator interaction. The URANS simulation for rigid blades predicts a dominant frequency of the travelling vortices at a non-engine order at 2603 Hz, which matches with accurately the NSV frequency obtained from the rig testing.

The results from the fully coupled fluid structure simulation accurately captures the blade NSV that agrees with the measurement at the same predicted aerodynamic excitation frequency with rigid blades. The results of the comparison seems indicating that the NSV of this compressor is a LCO excited by aerodynamic forcing instead of being caused by

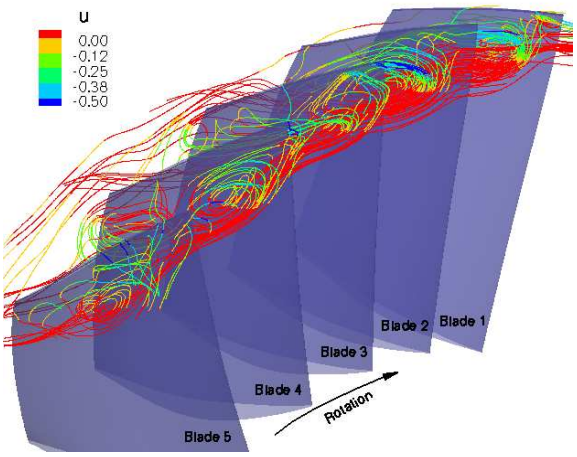

FIGURE 23: Structure of the RI in FSI simulation

flow phase locking to structural frequency. However, it may not be conclusive without simulating broader range of RPM and mass flow rate. In addition, the first bending vibration is predicted in the FSI with larger amplitude the 1st torsional mode NSV. The 1st bending vibration is not detected in the rig tests. The reason may be because the accurate mechanical damping is not known. In this study, all five modes use zero mechanical damping, which may artificially amplify the 1st bending mode. More research needs to be done to study different mechanical damping for each mode and their structural response.

Acknowledgments

We thank GE for approving publishing the results. We greatly appreciate the help of Gerardo "LC" Colmenero and Steve Manwaring at GE Aviation for providing the compressor geometry and testing data. The grants support from AFRL and the industrial partners of GUIde Consortium, 10-AFRL-1024 and 09-GUIDE-1010, are acknowledged. The numerical simulations are conducted at the Center for Computational Sciences at the University of Miami and Air Force Research Lab DoD High Performance Computing Centers.

REFERENCES

[1] M. Baumgartner, F. Kameier, and J. Hourmouziadis, "Non-Engine Order Blade Vibration in a High Pressure Compressor." ISABE, Twelfth International Symposium on Airbreathing Engines, Melbourne, Australia, 10-15, 1995.

[2] R. Kielb, J. Thomas, P. barter, and K. Hall, "Blade Excitation by Aerodynamic Instabilites - A Compressor Blade Study." ASME Paper No. GT-2003-38634, 2003.

[3] J. Marz, C. Hah, and W. Neise, "An Experimental and Numerical Investigation Into the Mechanisms of Rotating Instability," *Journal of Turbomachinery*, vol. 124, pp. 367–375, 2002.

[4] R. Mailach, I. Lehmann, and K. Vogeler, "Rotating Instabilites in an Axial Compressor Originating From the Fluctuating Blade Tip Vortex." ASME Paper No. GT-2003-38634, 2003.

[5] J. Thomassin, H. Vo, and N. Mureithi, "Blade Tip Clearance Flow and Compressor Nonsynchronous Vibrations: The Jet Core Feedback Theory as the Coupling Mechanism," *Journal of Turbomachinery*, vol. 131, pp. 11013–1–11013–9, 2009.

[6] J. Thomassin, H. Vo, and N. Mureithi, "The Tip Clearance Flow Resonance Behind Axial Compressor Nonsynchronous Vibration," *Journal of Turbomachinery*, vol. 133, pp. 041030–1–041030–10, 2011, doi:10.1115/1.4001368.

[7] A. Sanders, "Nonsynchronous Vibration(NSV) due to a Flow-Induced Aerodynamic Instability in a Composite Fan Stator," *Journal of Turbomachinery*, vol. 127, pp. 412–421, 2005.

[8] Vo, H.D., "Role of Tip Clearance Flow in Rotating Instabilities and Nonsynchronous Vibrations," *Journal of Propulsion and Power*, vol. 26, pp. 556–561, doi: 10.2514/1.26709, 2010.

[9] H.S. Im, and G.C. Zha, "Effects of Rotor Tip Clearance on Non-Synchronous Blade Vibration for an Axial Compressor." ASME GT2012-68148, 2012.

[10] H.S. Im, and G.C. Zha, "Simulation of Non-Synchronous Blade Vibration of an Axial Compressor Using a Fully Coupled Fluid/Strcuture Interaction." ASME GT2012-68150, 2012.

[11] S. Clark, R. Kielb, and K. Hall, "Developing a Reduced-Order Model to Understand Nonsynchronous Vibration (NSV) in Turbomachinery." ASME GT2012-68145, 2012.

[12] P.R. Spalart, W.H. Jou, M. Strelets, and S.R. Allmaras, "Comments on the Feasibility of LES for Wings, and on a Hybrid RANS/LES Approach." Advances in DNS/LES, 1st AFOSR Int. Conf. on DNS/LES, Greyden Press, Columbus, H., Aug. 4-8, 1997.

[13] G.C. Zha, Y.Q. Shen, and B.Y. Wang, "An Improved Low Diffusion E-CUSP Upwind Scheme ," *Journal of Computer and Fluids*, vol. 48, pp. 214–220, 2011, doi:10.1016/j.compfluid.2011.03.012.

[14] Y.Q. Shen, G.C. Zha, and B.Y. Wang, "Improvement of Stability and Accuracy of Implicit WENO Scheme," *AIAA Journal*, vol. 47, pp. 331–334, DOI:10.2514/1.37697, 2009.

[15] Y.Q. Shen, B.Y. Wang, and G.C. Zha, "Implicit WENO Scheme and High Order Viscous Formulas for Compressible Flows ." AIAA Paper 2007-4431, 2007.

[16] B. Wang, Z. Hu, and G. Zha, "A General Sub-Domain Boundary Mapping Procedure For Structured Grid CFD Parallel Computation," *AIAA Journal of Aerospace Computing, Information, and Communication*, vol. 5, pp. 425–447, 2008.

[17] H.-S. Im, X.-Y. Chen, and G.-C. Zha, " Detached Eddy Simulation of Transonic Rotor Stall Flutter Using a Fully Coupled Fluid-Structure Interaction." ASME GT2011-45437, ASME Turbo Expo 2011, Vancouver,

Canada, June 2011, 2011.
[18] H.S. Im, X.Y. Chen, and G.C. Zha, "Detached Eddy Simulation of Stall Inception for a Full Annulus Transonic Rotor," *Journal of Propulsion and Power*, vol. 28 (No. 4), pp. 782–798, doi: 10.2514/1.58970, 2012.
[19] H.S. Im, X.Y. Chen, and G.C. Zha, "Simulation of 3D Multistage Axial Compressor Using a Fully Conservative Sliding Boundary Condition." ASME IMECE2011-62049, International Mechanical Engineering Congress & Exposition, Denver, November 2011, 2011.